Research Article
Angewandte Chemie International Edition
www.angewandte.org
How to cite: Angew. Chem. Int. Ed. **2024**, e202413653
doi.org/10.1002/anie.202413653

Acidic Water Electrolysis | Hot Paper

Oxyanion Engineering on RuO_2 for Efficient Proton Exchange Membrane Water Electrolysis

Ying Duan+, Lin-Lin Wang+, Wen-Xing Zheng+, Xiao-Long Zhang, Xiao-Ran Wang, Guo-Jin Feng, Zi-You Yu,* and Tong-Bu Lu**

Abstract: In acidic proton exchange membrane water electrolysis (PEMWE), the anode oxygen evolution reaction (OER) catalysts rely heavily on the expensive and scarce iridium-based materials. Ruthenium dioxide (RuO_2) with lower price and higher OER activity, has been explored for the similar task, but has been restricted by the poor stability. Herein, we developed an anion modification strategy to improve the OER performance of RuO_2 in acidic media. The designed multicomponent catalyst based on sulfate anchored on RuO_2/MoO_3 displays a low overpotential of 190 mV at 10 $mA\,cm^{-2}$ and stably operates for 500 hours with a very low degradation rate of 20 $\mu V\,h^{-1}$ in acidic electrolyte. When assembled in a PEMWE cell, this catalyst as an anode shows an excellent stability at 500 $mA\,cm^{-2}$ for 150 h. Experimental and theoretical results revealed that MoO_3 could stabilize sulfate anion on RuO_2 surface to suppress its leaching during OER. Such MoO_3-anchored sulfate not only reduces the formation energy of *OOH intermediate on RuO_2, but also impedes both the surface Ru and lattice oxygen loss, thereby achieving the high OER activity and exceptional durability.

Introduction

The production of hydrogen (H_2) via water splitting using renewable energy sources offers a sustainable solution to carbon emissions and energy needs.[1–3] Among different water electrolysis technologies, acidic proton exchange membrane water electrolysis (PEMWE) exhibits many remarkable advantages, such as high operation current density, high hydrogen purity, low resistance loss, and compact device design.[1–5] There are substantial challenges to develop high-performance oxygen evolution reaction (OER) catalysts in the anode of PEMWE, due to its sluggish four-electron transfer and harshly acidic and oxidative environments.[6–8] For decades, Iridium (Ir) and its oxides have demonstrated considerable stability under such conditions, thus becoming the preferred choice as anode catalysts.[8–10] However, the high cost and extreme scarcity of Ir have posed a major barrier to the large-scale application of PEMWE. In recent years, ruthenium dioxide (RuO_2) with lower price and higher OER activity, has emerged as a promising alternative to Ir-based catalysts.[11–13] Unfortunately, the long-term stability of Ru-based OER catalysts remains a formidable challenge in acidic media.

Theoretically, the instability of RuO_2 during acidic OER is attributed to two primary reasons.[4,14–16] The first one is due to the lattice oxygen participation OER process, which results in the collapse of RuO_2 crystal structure.[14,17] The second one is the over-oxidation of RuO_2 into soluble high-valence H_2RuO_5 species, leading to the demetallation of surface Ru site.[4,18] To enhance the activity and stability of RuO_2-based electrocatalysts, various strategies have been proposed, including defect engineering,[19–21] interface designing,[22–24] strain tuning,[25–27] cation doping,[12,28–36] and others. In recent years, most studies have focused on using metal cation doping to regulate the chemical environments of Ru and O sites and optimize the adsorption energy of oxygenated intermediates (such as *OH, *O, and *OOH).[12,28,30–32,34–36] Besides the cation doping, the anion doping or modification has been reported as an efficient strategy to break the *OH/*OOH scaling relation, regulate the oxidation states of metal sites, and stabilize the lattice oxygen, thereby enhancing the OER performance of Ni/Fe-based catalysts in alkaline electrolytes.[37–40] We anticipate that the anion modified RuO_2 could decrease the intermediate formation energy and stabilize the Ru site and lattice oxygen to boost its OER activity and stability in acid.[41–42] However, the anion suffers from the serious loss during OER, and the robust anchoring of anion on RuO_2 is still highly required.

Herein, we reported an anion modification strategy to improve the OER performance of RuO_2 by developing a multicomponent catalyst based on sulfate anchored on RuO_2/MoO_3 (denoted as $RuO_2/MoO_3–SO_4$). This catalyst demonstrated outstanding OER activity and long-term stability in acidic electrolyte, thereby facilitating the successful demonstration of a high-performance electrolyzer under

---

[*] Y. Duan,+ L.-L. Wang,+ W.-X. Zheng,+ X.-R. Wang, G.-J. Feng, Prof. Z.-Y. Yu, Prof. T.-B. Lu
MOE International Joint Laboratory of Materials Microstructure, Institute for New Energy Materials and Low Carbon Technologies, School of Materials Science & Engineering, Tianjin University of Technology, 300384 Tianjin, China
E-mail: yuziyou@email.tjut.edu.cn
lutongbu@tjut.edu.cn

Dr. X.-L. Zhang
Division of Nanomaterials & Chemistry, Hefei National Research Center for Physical Sciences at the Microscale, University of Science and Technology of China, 230026 Hefei, China
E-mail: xlzhang0@ustc.edu.cn

[+] These authors contributed equally to this work.

realistic PEMWE operation. The notable performance could be attributed to the MoO_3-stabilized sulfate anion on RuO_2, which not only lowers the formation energy of *OOH from *O, thus improving the OER activity, but also hinders surface Ru demetallation and lattice oxygen loss to achieve the excellent durability.

Results and Discussion

We first performed DFT calculations to explore the effect of oxyanions on the energies for the OER and on the electronic structures of RuO_2. The slab model of RuO_2 (110) surface was constructed as the representative crystal surface for calculations.[12,29] In the outermost layer of the RuO_2 (110) surface, there are two types of Ru sites: the coordinatively unsaturated Ru sites (Ru_{cus}) and the fully coordinated bridge Ru (Ru_{bri}), with the former being the active sites for OER. We calculated the free energy of OER for RuO_2 via adsorbate evolution mechanism (AEM) pathway (Supporting Information, Figure S1), according to our ^{18}O isotope-labeled operando differential electrochemical mass spectrometry experiment (Supporting Information, Figure S2) and prior theoretical works.[12,43–44] Figure 1a reveals that the formation of *OOH from *O is kinetically hindered because of the highest energy barrier, in agreement with previous DFT studies.[12,30] Moreover, when different oxyanions including SeO_4, PO_4, and SO_4 ions are individually adsorbed onto the RuO_2 (110) surface (denoted as RuO_2–SeO_4, RuO_2–PO_4, and RuO_2–SO_4, respectively), the energies of this rate-determining step are reduced to 1.75, 1.70 and 1.62 eV, respectively, indicating the lowest formation energy of *OOH on RuO_2–SO_4 (Figure 1b; Supporting Information, Figure S3). The projected density of states (PDOS) of Ru sites revealed that they are sensitive to the different adsorbed oxyanions (Figure 1c). Compared with the RuO_2, the adsorbed oxyanions move the *d*-band center of Ru closer to the Fermi level in the order of $RuO_2 < RuO_2–SeO_4 < RuO_2–PO_4 < RuO_2–SO_4$, which corresponds to less e_g-filling of Ru antibonding state, thus leading to stronger *OOH adsorption.

The energy cost for Ru demetallation and O loss on the surface of RuO_2 and RuO_2–SO_4 were also calculated (Figure 1d; Supporting Information, Figure S4). We found that the energy cost for Ru demetallation increased from 1.62 eV for RuO_2 to 2.38 eV for RuO_2–SO_4, indicating an important role of SO_4 in stabilizing the surface Ru. In addition, the energy consumption of surface O loss for RuO_2 and RuO_2–SO_4 were calculated to be 3.13 and 3.56 eV, respectively. Consequently, our DFT calculations show that adsorption of SO_4 can improve the OER stability of RuO_2 by preventing both surface Ru demetallation and lattice oxygen loss. However, SO_4 is vulnerable during OER due to the weak bonding between the catalyst and SO_4 (Figure 1e). We therefore envisaged fixing acid-resistant metal oxide on RuO_2 surface to coordinate with the O atoms in SO_4, thus immobilizing SO_4 on the catalyst. Among the acid-resistant metal oxides proposed by Nørskov et al.,[45] MoO_3 possesses the strongest binding energy with sulfate (Figure 1e). Therefore, MoO_3 was selected as the oxide to anchor sulfate on the RuO_2 surface.

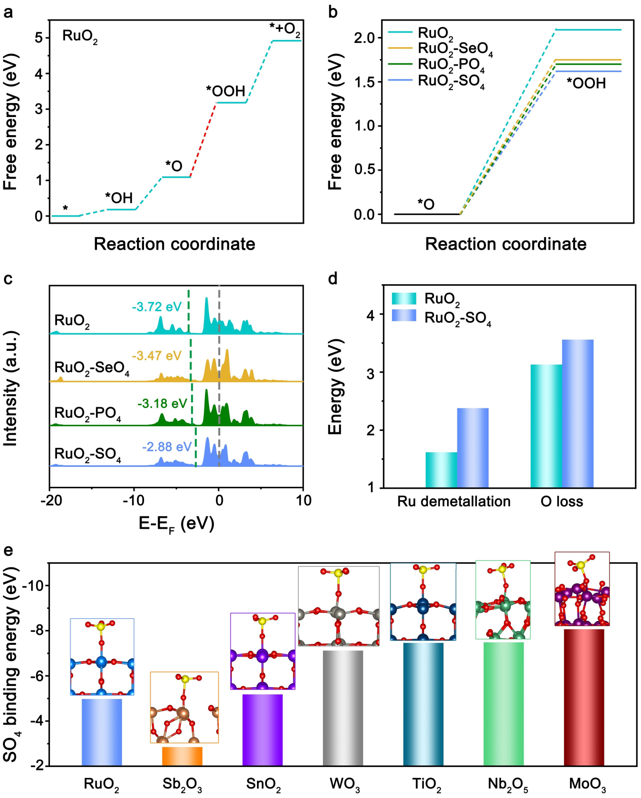

Figure 1. DFT calculations. a) Free energy change diagrams of OER on surfaces of RuO_2 (110). b) Free energy change of the formation of *OOH from *O on the surface of RuO_2, RuO_2–SeO_4, RuO_2-PO_4, and RuO_2–SO_4. c) Calculated PDOS of RuO_2, RuO_2–SeO_4, RuO_2-PO_4, and RuO_2–SO_4 with the Fermi level aligned at 0 eV. Green dashed line located at the d-band center for all models. d) Calculated energy cost for Ru demetallation and O loss on the surface of RuO_2 and RuO_2–SO_4. e) Calculated sulfate binding energy of RuO_2, Sb_2O_3, SnO_2, WO_3, TiO_2, Nb_2O_5 and MoO_3.

The above DFT calculations suggest that MoO_3 anchored sulfate on the RuO_2 surface holds the possibility of enhancing the activity and stability of RuO_2 for acidic OER. We thereby designed a multicomponent OER catalyst based on RuO_2/MoO_3–SO_4 and its preparation process was illustrated in Figure 2a. We first synthesized MoS_2 nanosheets as the Mo and S precursors using a simple hydrothermal reaction (see the Experimental section; Supporting Information, Figure S5). Then RuO_xH_y/MoS_2 precursor was obtained through a hydrothermal treatment of $RuCl_3$ aqueous solution and MoS_2 nanosheets at 120 °C. Consequently, the resulted powder was annealed at 400 °C in air atmosphere to obtain RuO_2/MoO_3–SO_4 catalyst (Figure 2a). During the annealing process, RuO_xH_y and MoS_2 were in situ thermally converted to RuO_2 and sulfate anchored MoO_3, respectively.

As imaged by transmission electron microscopy (TEM), RuO_2/MoO_3–SO_4 catalyst was composed of small nanoparticles (Figure 2b and Supporting Information, Figure S6). X-ray diffraction (XRD) pattern of RuO_2/MoO_3–SO_4 catalyst showed the typical diffraction peaks from rutile RuO_2

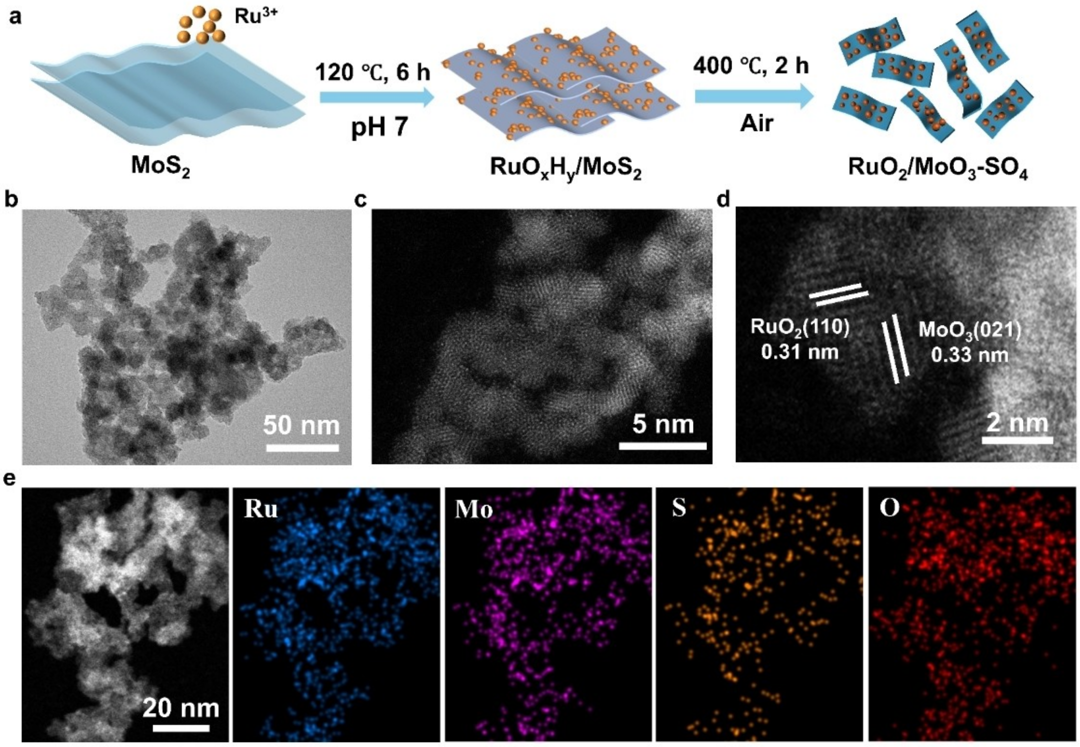

Figure 2. Synthesis and characterization of RuO_2/MoO_3–SO_4 catalyst. a) Schematic illustrating the synthesis of RuO_2/MoO_3–SO_4. b) TEM image of RuO_2/MoO_3–SO_4. c), d) HAADF-STEM images of RuO_2/MoO_3–SO_4. e) EDS elemental mappings of RuO_2/MoO_3–SO_4.

(JCPDS no. 40-1290) and orthorhombic MoO_3 (JCPDS no. 05-0508) without any impurity (Supporting Information, Figure S7). The molar ratio of Ru:Mo:S in RuO_2/MoO_3–SO_4 was determined to be 3.9:1:0.8 from inductively coupled plasma mass spectroscopy (ICP-MS) measurement. High-angle annular dark field-scanning transmission electron microscopy (HAADF-STEM) images gave the distinct RuO_2/MoO_3 with resolved lattice planes of RuO_2(110) and MoO_3(021) (Figure 2c, d). Energy-dispersive X-ray spectroscopy (EDS) elemental mappings (Figure 2e) demonstrated the homogeneous distribution of Ru, Mo, S and O elements. Other control samples, including RuO_2/MoO_3 without anchored sulfate (RuO_2/MoO_3), RuO_2 with anchored sulfate (RuO_2–SO_4), and pure RuO_2 (RuO_2), were also synthesized for comparison (Supporting Information, Figures S8 and S9).

We first investigated the acidic OER performance of RuO_2/MoO_3–SO_4 catalyst and other control samples on a rotating disk electrode (RDE) in a conventional three-electrode construction. Linear sweep voltammetry (LSV) curves in Figure 3a show that RuO_2/MoO_3–SO_4 had the earliest onset potential at 1.37 V versus reversible hydrogen electrode (RHE), beyond which a sharp increase of OER current was observed. To reach a current density of $10\ \mathrm{mA\,cm^{-2}}$, commercial RuO_2 (Com-RuO_2, Supporting Information, Figure S10) required a high overpotential of 317 mV, consistent with many previous reports.[12,25,31–32] The required overpotentials of other catalysts followed an order of RuO_2/MoO_3–SO_4 (190 mV) $<$ RuO_2–SO_4 (233 mV) $<$ RuO_2 (251 mV), indicating the best OER activity of RuO_2/MoO_3–SO_4 catalyst (Figure 3a). RuO_2/MoO_3 catalyst has the similar OER activity with RuO_2, suggesting the negligible contribution of MoO_3 on pure RuO_2 (Supporting Information, Figure S11). Tafel analysis (Figure 3b) revealed that RuO_2/MoO_3–SO_4 had a small slope of $38\ \mathrm{mV\,dec^{-1}}$, much lower than that of RuO_2–SO_4 ($52\ \mathrm{mV\,dec^{-1}}$), RuO_2 ($58\ \mathrm{mV\,dec^{-1}}$), and Com-$RuO_2$ ($71\ \mathrm{mV\,dec^{-1}}$), implying a lower OER overpotential needed for RuO_2/MoO_3–SO_4 at higher current densities. Further electrochemical impedance spectroscopy (EIS) tests were used to determine the charge transfer resistance (R_{ct}). The smallest R_{ct} of $\sim 6\ \Omega$ was achieved on RuO_2/MoO_3–SO_4 (Figure 3c), confirming its fast charge transfer kinetics, in line with the above Tafel analysis.

To further investigate the origin of high OER activity of RuO_2/MoO_3–SO_4 catalyst, we performed the electrochemically active surface area (ECSA) tests (Supporting Information, Figures S12 and S13). Compared to Com-RuO_2, the high ECSA values for our as-synthesized catalysts could be attributed to the particle size effect. Especially, RuO_2/MoO_3–SO_4 delivered the largest ECSA of $214.3\ \mathrm{cm^2}$, nearly 2-fold higher than that of RuO_2, showing that the density of active sites could be increased by the incorporation of MoO_3 and sulfate anions. When we calculated ECSA-normalized OER activity (Figure 3d; Supporting Information, Figure S13), RuO_2/MoO_3–SO_4 still has the overwhelming activity over other samples, suggesting the intrinsically active sites not only the increased surface areas working on

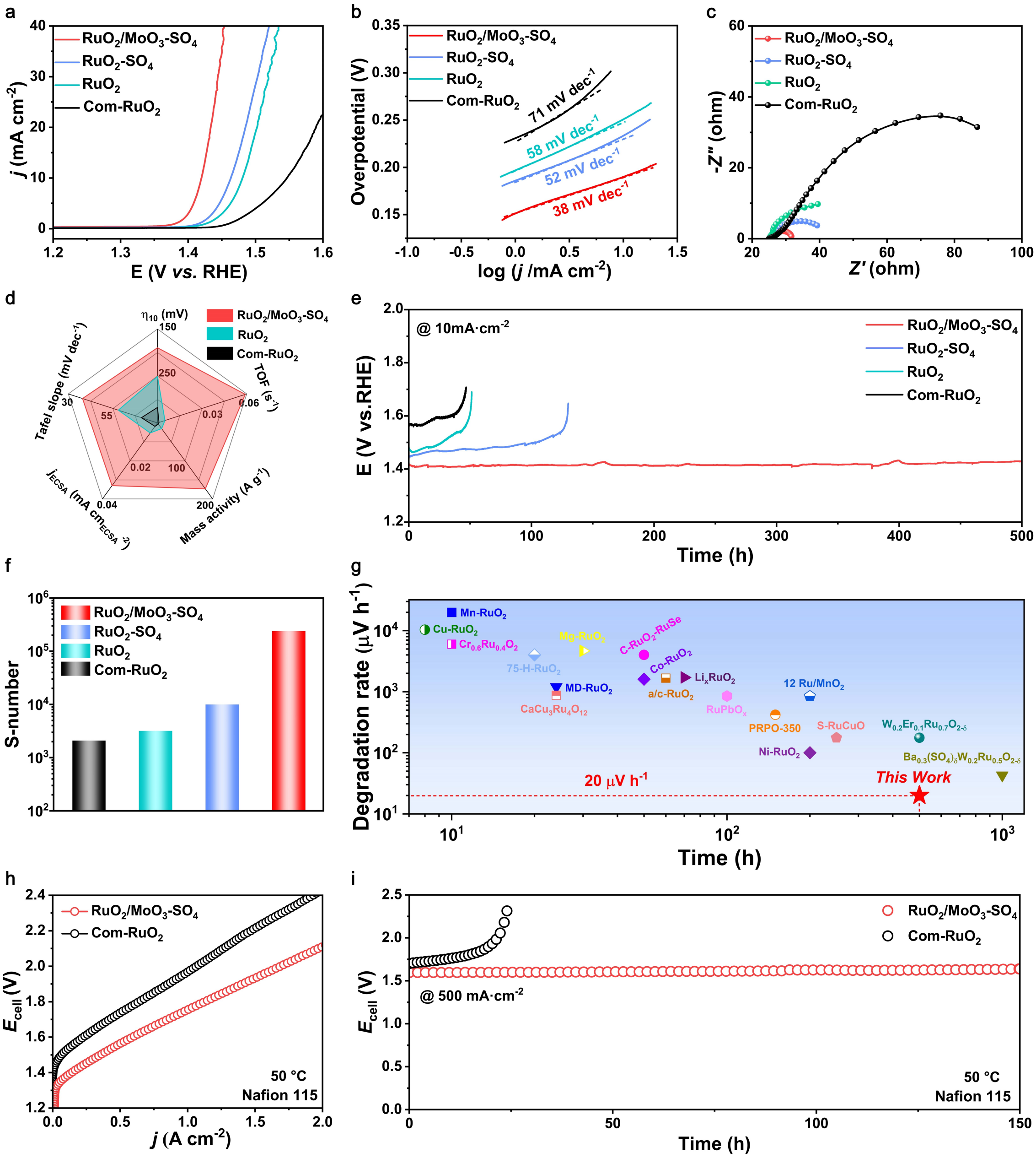

Figure 3. Electrocatalytic performance. a)–c) LSV curves (a), Tafel plots (b) and EIS plot (c) of different catalysts in O_2-saturated 0.1 M $HClO_4$. d) Radar diagram of some key OER activity metrics of different catalysts. e) Chronopotentiometry curves at 10 mA cm^{-2} of different catalysts. f) The calculated S-number of different catalysts. g) Comparison of degradation rate and stability time of RuO_2/MoO_3–SO_4 with other reported Ru-based catalysts in acidic media. h) Polarization curves of PEMWE device using RuO_2/MoO_3–SO_4 or Com-RuO_2 as anode catalyst. i) Chronopotentiometry curves of PEMWE device using RuO_2/MoO_3–SO_4 or Com-RuO_2 as anode catalyst operated at 500 mA cm^{-2} and 50 °C.

RuO_2/MoO_3–SO_4 catalyst for the impressive performance. Figure 3d also compares various significant activity metrics of distinct catalysts. RuO_2/MoO_3–SO_4 generates a turnover frequency (TOF) of 0.059 s^{-1} at 1.45 V versus RHE, which is 12 and 59 times higher than those of RuO_2 and Com-RuO_2, respectively. Furthermore, the mass activity of RuO_2/MoO_3–SO_4 normalized by Ru loading mass, is significantly higher than those of RuO_2 and Com-RuO_2 (Figure 3d and Supporting Information, Figure S14).

Apart from activity, the durability of catalysts may play an even more critical role for the practical application of water splitting. We examined the OER stability by performing the chronopotentiometry tests at 10 mA cm^{-2} in acidic electrolytes (Figure 3e). Com-RuO_2 and as-prepared RuO_2 exhibited a very poor stability to drastically degrade within 50 h. The poor stability for Com-RuO_2 was also observed in previous works.[12,30–31,34] RuO_2–SO_4 could moderately extend the durability for about 110 h. More impressively, RuO_2/MoO_3–SO_4 catalyst presented a very excellent stability with a negligible voltage increase of mere ~10 mV after a continuous 500 h test (red curve, Figure 3e), yielding a very low degradation rate of 20 $\mu V h^{-1}$ (Supporting Information, Figure S15). The control experiment revealed that the physically adsorbed sulfate anion has little lifting effect on the stability of RuO_2 (Supporting Information, Figure S16). We further quantified the dissolved S amount by ICP-MS test (Supporting Information, Table S1), yielding an S loss of 15.2 % for RuO_2/MoO_3–SO_4 and 66.7 % for RuO_2–SO_4 after stability tests, indicating the incorporation of MoO_3 could greatly fix the sulfate on the RuO_2 surface. Meanwhile, RuO_2/MoO_3–SO_4 exhibits a small dissolution of 3.2 % for Ru and 5.4 % for Mo after 500 h. We thus calculated the stability number (S-number, Supporting Information, Table S1) based on the dissolved Ru amount proposed by Geiger et al.,[46] and the S-number of RuO_2/MoO_3–SO_4 at 500 h was determined to be 2.4×10^5, 24, 75, and 114 times higher than that of RuO_2–SO_4, RuO_2, and Com-RuO_2, respectively (Figure 3f). Based on these results, we can highlight that the high OER activity, long durability, and low degradation rate render our RuO_2/MoO_3–SO_4 catalyst to represent the best Ru-based OER catalysts in acidic electrolytes reported as yet (Figure 3g and Supporting Information, Table S2).

Motivated by the above results of three-electrode test, we proceeded to construct a PEMWE device using RuO_2/MoO_3–SO_4 or Com-RuO_2 as the anode catalyst (Supporting Information, Figure S17). The assembled electrolyser was supplied with pure deionized water as reactant, the used membrane was Nafion 115, and the operation temperature was set at 50 °C. The polarization curves presented in Figure 3h illustrate that the RuO_2/MoO_3–SO_4 catalyst neces-

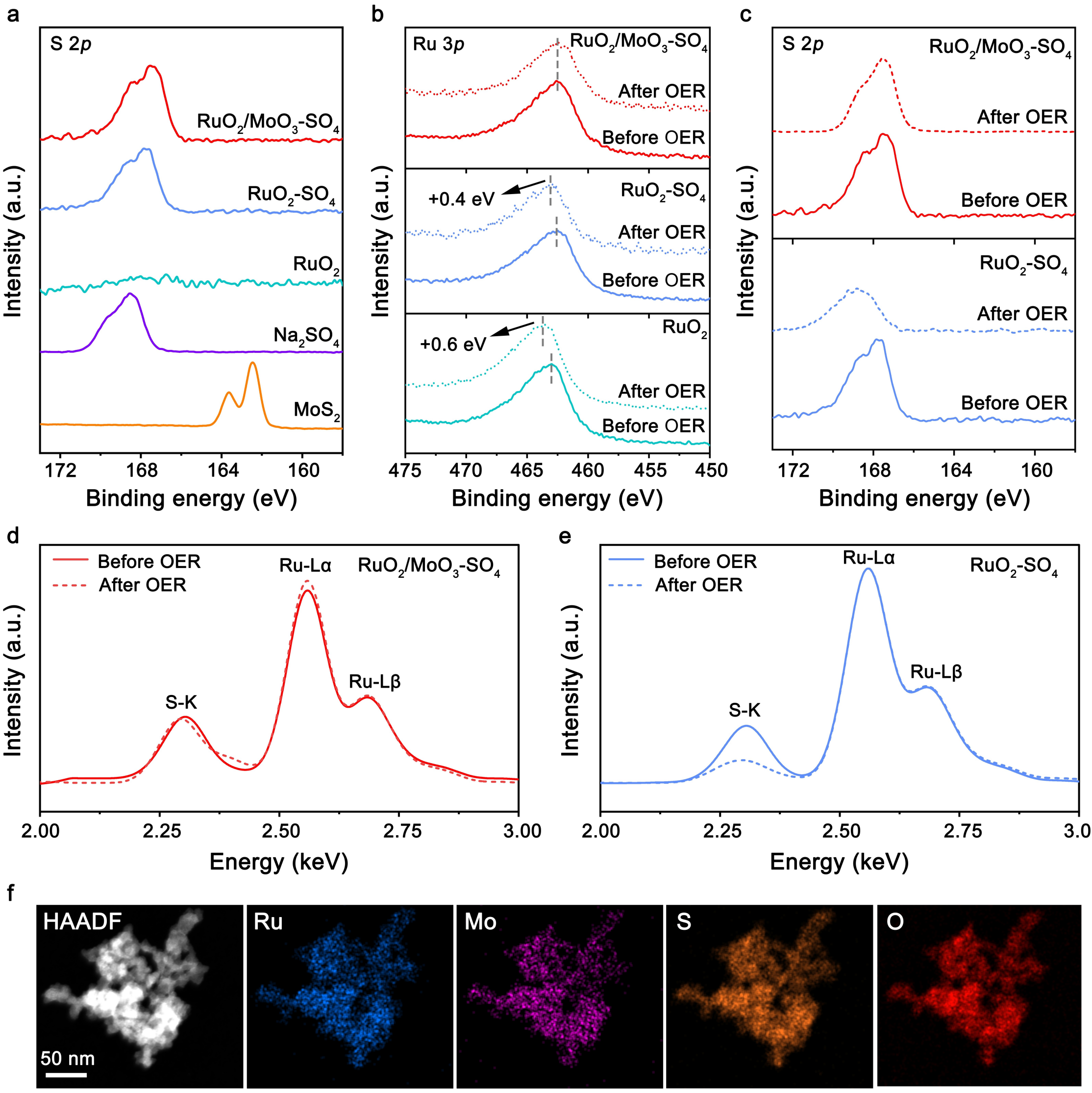

Figure 4. Stability study after OER. a) S 2*p* XPS spectra of MoS_2, Na_2SO_4, RuO_2, RuO_2–SO_4, and RuO_2/MoO_3–SO_4. b) Ru $3p_{3/2}$ XPS spectra of RuO_2, RuO_2–SO_4 and RuO_2/MoO_3–SO_4 catalyst before and after OER. c) S 2*p* XPS spectra of RuO_2–SO_4 and RuO_2/MoO_3–SO_4 catalyst before and after OER. d), e) EDS spectra of RuO_2/MoO_3–SO_4 (d) and RuO_2–SO_4 (e) before and after OER. f) EDS elemental mappings of RuO_2/MoO_3–SO_4 after OER. The catalyst after OER here was obtained by performing at 1.45 V for 48 h in 0.1 M $HClO_4$.

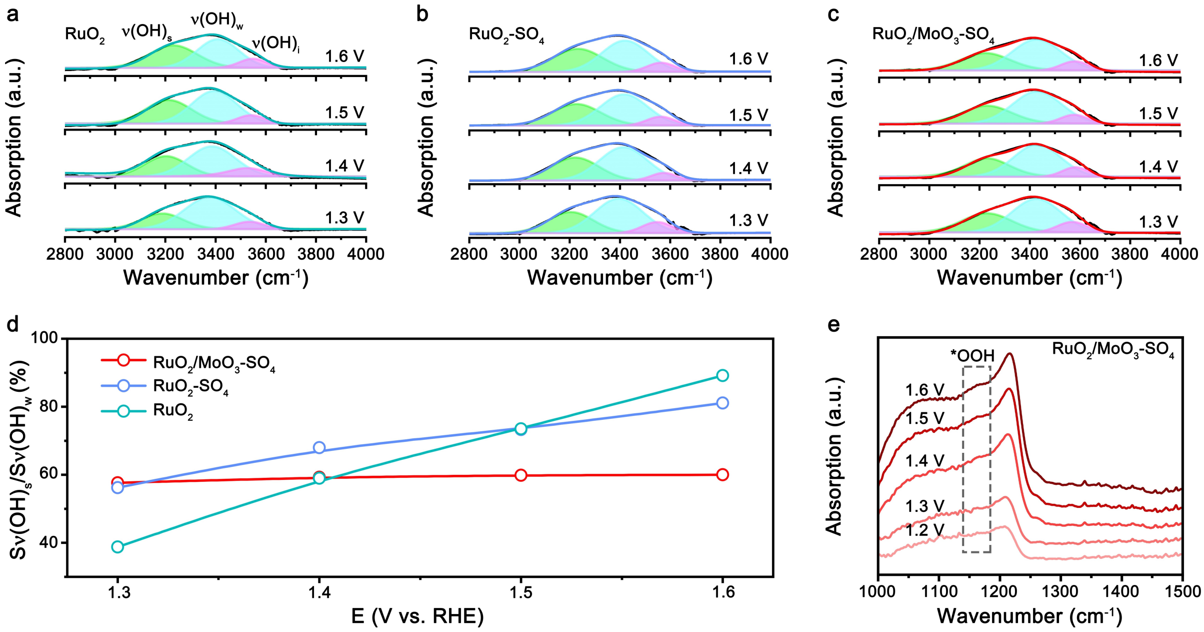

Figure 5. In situ spectroscopy measurements. a)–c) In situ ATR-SEIRAS spectra recorded between 2800 and 4000 cm^{-1} on RuO$_2$ (a), RuO$_2$–SO$_4$ (b) and RuO$_2$/MoO$_3$–SO$_4$ (c) at different applied potentials. d) The area ratio of $\upsilon(OH)_s/\upsilon(OH)_w$ on RuO$_2$, RuO$_2$–SO$_4$ and RuO$_2$/MoO$_3$–SO$_4$. e) In situ ATR-SEIRAS spectra recorded between 1000 and 1500 cm^{-1} on RuO$_2$/MoO$_3$–SO$_4$ at different applied potentials. The broad peak at ~1220 cm^{-1} was assigned to the Si–O–Si vibration from the ATR crystal.

sitates a cell voltage of 1.75 V at 1 A cm^{-2} without the iR correction, which is notably 230 mV lower than the voltage required by Com-RuO$_2$. Remarkably, the RuO$_2$/MoO$_3$–SO$_4$ catalyst can operate consistently at 500 mA cm^{-2} for 150 h, with a small potential increase of merely 42 mV. This is a stark contrast to the Com-RuO$_2$, which deactivates within just 20 hours (Figure 3i). The performance of the RuO$_2$/MoO$_3$–SO$_4$ catalyst in PEMWE outperforms the majority of Ru-based catalysts reported previously (Supporting Information, Table S3), thereby indicating its potential for industrial-scale water electrolysis.

We performed X-ray photoelectron spectroscopy (XPS) to characterize the surface chemical states of S element. The obvious S 2*p* signals were observed on RuO$_2$–SO$_4$ and RuO$_2$/MoO$_3$–SO$_4$ samples from their survey XPS spectra (Supporting Information, Figure S18). In order to further investigate the S chemical states, we also measured S XPS spectra of Na$_2$SO$_4$ and MoS$_2$ (Figure 4a), which as the reference samples have the typical peaks of SO$_4^{2-}$ and S^{2-} anions, respectively. RuO$_2$–SO$_4$ and RuO$_2$/MoO$_3$–SO$_4$ samples exhibit the characteristic features of SO$_4^{2-}$ anions, which are similar to that of Na$_2$SO$_4$, but are greatly distinctive that of MoS$_2$. These results demonstrated that the SO$_4^{2-}$ anions were successfully attached to the RuO$_2$ and RuO$_2$/MoO$_3$ through our synthetic method.

We next combined multiple characterization techniques to examine the structural stability of the studied catalysts. The surface morphology and crystalline phase of RuO$_2$/MoO$_3$–SO$_4$ catalyst after OER still kept its pristine state (Supporting Information, Figures S19 and S20). Further high-resolution Ru XPS spectra show that Ru 3*p* binding energies for RuO$_2$ and RuO$_2$–SO$_4$ after OER tests experience a positive shift of 0.6 and 0.4 eV, respectively, in comparison to its pre-reaction state (Figure 4b and Supporting Information, Figure S21), indicating the increased Ru valence states for these catalysts.[31,42] By contrast, RuO$_2$/MoO$_3$–SO$_4$ catalyst exhibited the unchanged peak position after OER, implying that sulfate anion and MoO$_3$ together safeguard RuO$_2$/MoO$_3$–SO$_4$ catalyst to prevent Ru sites from over-oxidation. Figure 4c shows the S 2*p* XPS spectra of RuO$_2$–SO$_4$ and RuO$_2$/MoO$_3$–SO$_4$ catalyst before and after OER tests. The surface sulfate anion of RuO$_2$/MoO$_3$–SO$_4$ catalyst can still maintain its initial coverage and chemical state after OER, whereas RuO$_2$–SO$_4$ catalyst undergoes a severe loss of sulfate anion.

We further performed the EDS analysis to detect the variation of sulfate amount after stability tests. The RuO$_2$/MoO$_3$–SO$_4$ catalyst shows a negligible change of S/Ru ratio after OER (Figure 4d and Supporting Information, Figure S22). By contrast, the S/Ru ratio in RuO$_2$–SO$_4$ decreases from its original value of 0.19 to 0.06 after OER (Figure 4e and Supporting Information, Figure S22), indicating the severe loss of sulfate for RuO$_2$–SO$_4$ catalyst. They agree well with our EDS elemental mapping studies shown in Figures 2e, 4f and Supporting Information, Figure S23. These above observations suggest that MoO$_3$ contributes to the stabilization of sulfate on the catalyst surface.

Now, we turned to use in situ attenuated total reflection surface-enhanced infrared absorption spectroscopy (ATR-SEIRAS) to uncover the dynamic structure evolution under OER conditions. The spectra with wavenumbers from ~3000 to ~3700 cm^{-1} could provide information about the O–H stretching modes of the interfacial H-bonded water network at OER-relevant potentials (see Methods; Figure 5a–c).

Using Gaussian fitting, the O–H stretching peaks could be consistently deconvoluted into three components:[47–48] isolated non-H-bonded water with free O–H bonds ($\upsilon(OH)_i$ at ~3600 cm^{-1}), trihedral H-bonded water with relatively weak O–H bonds ($\upsilon(OH)_w$ at ~3400 cm^{-1}), and tetrahedral H-bonded water with strong O–H bonds ($\upsilon(OH)_s$ at ~3200 cm^{-1}). Accordingly, $\upsilon(OH)_s$ and $\upsilon(OH)_w$ are related to the combination of O–H bond with unsaturated Ru site and lattice oxygen of catalyst, respectively.[42,49] As the applied positive bias was increased, a rapid increase of $\upsilon(OH)_s/\upsilon(OH)_w$ area ratio was observed on RuO_2 (Figure 5d). This surge is attributed to the formation of unsaturated Ru sites resulting from the over-oxidation of lattice oxygen. Conversely, on RuO_2–SO_4, the area ratio of $\upsilon(OH)_s/\upsilon(OH)_w$ increased slowly, particularly on RuO_2/MoO_3–SO_4, where the area ratio of $\upsilon(OH)_s/\upsilon(OH)_w$ remained nearly constant during acidic OER (Figure 5d). This further suggests that the presence of MoO_3 could stabilize sulfate on the RuO_2 surface, and thus the anchored sulfate protects the lattice oxygen and prevents the formation of oxygen vacancies, consistent with the above DFT calculation (Figure 1d).

To further analyze intermediates during acidic OER, in situ ATR-SEIRAS was recorded between 1000 and 1500 cm^{-1} on our studied catalysts under varying biases. As depicted in Figure 5e, RuO_2/MoO_3–SO_4 catalyst display a distinct peak at approximately 1155 cm^{-1} from 1.4 V to 1.6 V versus RHE, indicative of the *OOH intermediate.[32,50] In contrast, the ATR-SEIRAS spectra of other catalysts did not exhibit the obvious *OOH signal peak (Supporting Information, Figure S24), suggesting that MoO_3 anchoring sulfate promotes the formation of *OOH and thus improves the OER activity

Conclusion

In summary, we developed an anion modification strategy for RuO_2/MoO_3–SO_4 as an efficient and durable OER catalyst in acidic electrolyte. This notable performance is attributed to the MoO_3-protected sulfate anion on RuO_2, which can decrease the energy barrier of the formation of *OOH from *O and thus improve the OER activity. Moreover, it further stabilizes the surface Ru and lattice O of RuO_2 during acidic OER, guaranteeing the OER stability. Overall, this work presents a successful strategy for the rational design of high-performance ruthenium-based acidic OER catalysts for the future application in practical PEMWE technology.

Acknowledgments

This work was supported by National Key R&D Program of China (2022YFA1502902), and National Natural Science Foundation of China (21931007, 22375146, and 22109149).

Conflict of Interest

The authors declare no conflict of interest.

Data Availability Statement

The data that support the findings of this study are available in the supplementary material of this article.

Keywords: proton exchange membrane water electrolysis · oxygen evolution reaction · RuO_2 · anion modification strategy · acidic media

---

[1] M. Carmo, D. L. Fritz, J. Mergel, D. Stolten, *Int. J. Hydrogen Energy* **2013**, *38*, 4901–4934.

[2] Z.-Y. Yu, Y. Duan, X.-Y. Feng, X. Yu, M.-R. Gao, S.-H. Yu, *Adv. Mater.* **2021**, *33*, 2007100.

[3] L. Chong, G. Gao, J. Wen, H. Li, H. Xu, Z. Green, J. D. Sugar, A. J. Kropf, W. Xu, X.-M. Lin, H. Xu, L.-W. Wang, D.-J. Liu, *Science* **2023**, *380*, 609–616.

[4] T. Reier, H. N. Nong, D. Teschner, R. Schlögl, P. Strasser, *Adv. Energy Mater.* **2017**, *7*, 1601275.

[5] C. Spoeri, J. T. H. Kwan, A. Bonakdarpour, D. Wilkinson, P. Strasser, *Angew. Chem. Int. Ed.* **2017**, *56*, 5994–6021.

[6] Y. Lin, Y. Dong, X. Wang, L. Chen, *Adv. Mater.* **2022**, *35*, 2210565.

[7] L. C. Seitz, C. F. Dickens, K. Nishio, Y. Hikita, J. Montoya, A. Doyle, C. Kirk, A. Vojvodic, H. Y. Hwang, J. K. Norskov, T. F. Jaramillo, *Science* **2016**, *353*, 1011–1014.

[8] Y.-R. Zheng, J. Vernieres, Z. Wang, K. Zhang, D. Hochfilzer, K. Krempl, T.-W. Liao, F. Presel, T. Altantzis, J. Fatermans, S. B. Scott, N. M. Secher, C. Moon, P. Liu, S. Bals, S. Van Aert, A. Cao, M. Anand, J. K. Nørskov, J. Kibsgaard, I. Chorkendorff, *Nat. Energy* **2021**, *7*, 55–64.

[9] A. Li, S. Kong, K. Adachi, H. Ooka, K. Fushimi, Q. Jiang, H. Ofuchi, S. Hamamoto, M. Oura, K. Higashi, T. Kaneko, T. Uruga, N. Kawamura, D. Hashizume, R. Nakamura, *Science* **2024**, *384*, 666–670.

[10] S. Hao, H. Sheng, M. Liu, J. Huang, G. Zheng, F. Zhang, X. Liu, Z. Su, J. Hu, Y. Qian, L. Zhou, Y. He, B. Song, L. Lei, X. Zhang, S. Jin, *Nat. Nanotechnol.* **2021**, *16*, 1371–1377.

[11] Z. Shi, J. Li, Y. Wang, S. Liu, J. Zhu, J. Yang, X. Wang, J. Ni, Z. Jiang, L. Zhang, Y. Wang, C. Liu, W. Xing, J. Ge, *Nat. Commun.* **2023**, *14*, 843.

[12] Z.-Y. Wu, F.-Y. Chen, B. Li, S.-W. Yu, Y. Z. Finfrock, D. M. Meira, Q.-Q. Yan, P. Zhu, M.-X. Chen, T.-W. Song, Z. Yin, H.-W. Liang, S. Zhang, G. Wang, H. Wang, *Nat. Mater.* **2023**, *22*, 100–108.

[13] C. Wang, L. Jin, H. Shang, H. Xu, Y. Shiraishi, Y. Du, *Chin. Chem. Lett.* **2021**, *32*, 2108–2116.

[14] G. Zhao, W. Guo, M. Shan, Y. Fang, G. Wang, M. Gao, Y. Liu, H. Pan, W. Sun, *Adv. Mater.* **2024**, *36*, 2404213.

[15] Q. Wu, R. Zhou, Z. Yao, T. Wang, Q. Li, *Chin. Chem. Lett.* **2024**, *35*, 109416.

[16] F. Hess, *Curr. Opin. Electrochem.* **2023**, *41*, 101349.

[17] W. He, X. Tan, Y. Guo, Y. Xiao, H. Cui, C. Wang, *Angew. Chem. Int. Ed.* **2024**, *63*, e202405798.

[18] D. Chen, R. Yu, K. Yu, R. Lu, H. Zhao, J. Jiao, Y. Yao, J. Zhu, J. Wu, S. Mu, *Nat. Commun.* **2024**, *15*, 3928.

[19] Z. L. Zhao, Q. Wang, X. Huang, Q. Feng, S. Gu, Z. Zhang, H. Xu, L. Zeng, M. Gu, H. Li, *Energy Environ. Sci.* **2020**, *13*, 5143–5151.

[20] L. Zhang, H. Jang, H. Liu, M. G. Kim, D. Yang, S. Liu, X. Liu, J. Cho, *Angew. Chem. Int. Ed.* **2021**, *60*, 18821–18829.
[21] R. Ge, L. Li, J. Su, Y. Lin, Z. Tian, L. Chen, *Adv. Energy Mater.* **2019**, *9*, 1901313.
[22] Y. Hao, S. F. Hung, C. Tian, L. Wang, Y. Y. Chen, S. Zhao, K. S. Peng, C. Zhang, Y. Zhang, C. H. Kuo, H. Y. Chen, S. Peng, *Angew. Chem. Int. Ed.* **2024**, *63*, e202402018.
[23] L. Zhou, Y. Shao, F. Yin, J. Li, F. Kang, R. Lv, *Nat. Commun.* **2023**, *14*, 7644.
[24] X. Wang, X. Wan, X. Qin, C. Chen, X. Qian, Y. Guo, Q. Xu, W.-B. Cai, H. Yang, K. Jiang, *ACS Catal.* **2022**, *12*, 9437–9445.
[25] Y. Yao, S. Hu, W. Chen, Z.-Q. Huang, W. Wei, T. Yao, R. Liu, K. Zang, X. Wang, G. Wu, W. Yuan, T. Yuan, B. Zhu, W. Liu, Z. Li, D. He, Z. Xue, Y. Wang, X. Zheng, J. Dong, C.-R. Chang, Y. Chen, X. Hong, J. Luo, S. Wei, W.-X. Li, P. Strasser, Y. Wu, Y. Li, *Nat. Catal.* **2019**, *2*, 304–313.
[26] Y. Xu, Z. Mao, J. Zhang, J. Ji, Y. Zou, M. Dong, B. Fu, M. Hu, K. Zhang, Z. Chen, S. Chen, H. Yin, P. Liu, H. Zhao, *Angew. Chem. Int. Ed.* **2024**, *63*, e202316029.
[27] Y. Qin, T. Yu, S. Deng, X.-Y. Zhou, D. Lin, Q. Zhang, Z. Jin, D. Zhang, Y.-B. He, H.-J. Qiu, L. He, F. Kang, K. Li, T.-Y. Zhang, *Nat. Commun.* **2022**, *13*, 3784.
[28] D. Zhang, M. Li, X. Yong, H. Song, G. I. N. Waterhouse, Y. Yi, B. Xue, D. Zhang, B. Liu, S. Lu, *Nat. Commun.* **2023**, *14*, 2517.
[29] S. Jianwei, G. Ruixiang, J. Kemin, D. Yan, H. Fei, T. Ziqi, C. Guoxin, C. Liang, *Adv. Mater.* **2018**, *30*, 1801351.
[30] L. Li, G. Zhang, C. Zhou, F. Lv, Y. Tan, Y. Han, H. Luo, D. Wang, Y. Liu, C. Shang, L. Zeng, Q. Huang, R. Zeng, N. Ye, M. Luo, S. Guo, *Nat. Commun.* **2024**, *15*, 4974.
[31] P. Sun, Z. Qiao, X. Dong, R. Jiang, Z.-T. Hu, J. Yun, D. Cao, *J. Am. Chem. Soc.* **2024**, *146*, 15515–15524.
[32] H. Liu, Z. Zhang, J. Fang, M. Li, M. G. Sendeku, X. Wang, H. Wu, Y. Li, J. Ge, Z. Zhuang, D. Zhou, Y. Kuang, X. Sun, *Joule* **2023**, *7*, 558–573.
[33] S. Hao, M. Liu, J. Pan, X. Liu, X. Tan, N. Xu, Y. He, L. Lei, X. Zhang, *Nat. Commun.* **2020**, *11*, 5368.
[34] H. Jin, X. Liu, P. An, C. Tang, H. Yu, Q. Zhang, H.-J. Peng, L. Gu, Y. Zheng, T. Song, K. Davey, U. Paik, J. Dong, S.-Z. Qiao, *Nat. Commun.* **2023**, *14*, 354.
[35] L. Wu, Q. Liang, J. Zhao, J. Zhu, H. Jia, W. Zhang, P. Cai, W. Luo, *Chin. J. Catal.* **2023**, *55*, 182–190.
[36] Y. Wang, R. Yang, Y. Ding, B. Zhang, H. Li, B. Bai, M. Li, Y. Cui, J. Xiao, Z.-S. Wu, *Nat. Commun.* **2023**, *14*, 1412.
[37] J. N. Hausmann, P. W. Menezes, *Angew. Chem. Int. Ed.* **2022**, *61*, e202207279.
[38] Y. Shi, W. Du, W. Zhou, C. Wang, S. Lu, S. Lu, B. Zhang, *Angew. Chem. Int. Ed.* **2020**, *59*, 22470–22474.
[39] L. Yu, L. Wu, B. McElhenny, S. Song, D. Luo, F. Zhang, Y. Yu, S. Chen, Z. Ren, *Energy Environ. Sci.* **2020**, *13*, 3439–3446.
[40] T. Zhang, Y. Liu, L. Tong, J. Yu, S. Lin, Y. Li, H. J. Fan, *ACS Nano* **2023**, *17*, 6770–6780.
[41] Y. Xue, J. Fang, X. Wang, Z. Xu, Y. Zhang, Q. Lv, M. Liu, W. Zhu, Z. Zhuang, *Adv. Funct. Mater.* **2021**, *31*, 2101405.
[42] Y. Xue, J. Zhao, L. Huang, Y.-R. Lu, A. Malek, G. Gao, Z. Zhuang, D. Wang, C. T. Yavuz, X. Lu, *Nat. Commun.* **2023**, *14*, 8093.
[43] K. A. Stoerzinger, O. Diaz-Morales, M. Kolb, R. R. Rao, R. Frydendal, L. Qiao, X. R. Wang, N. B. Halck, J. Rossmeisl, H. A. Hansen, T. Vegge, I. E. L. Stephens, M. T. M. Koper, Y. Shao-Horn, *ACS Energy Lett.* **2017**, *2*, 876–881.
[44] R. R. Rao, M. J. Kolb, N. B. Halck, A. F. Pedersen, A. Mehta, H. You, K. A. Stoerzinger, Z. Feng, H. A. Hansen, H. Zhou, L. Giordano, J. Rossmeisl, T. Vegge, I. Chorkendorff, I. E. L. Stephens, Y. Shao-Horn, *Energy Environ. Sci.* **2017**, *10*, 2626–2637.
[45] Z. Wang, Y.-R. Zheng, I. Chorkendorff, J. K. Nørskov, *ACS Energy Lett.* **2020**, *5*, 2905–2908.
[46] S. Geiger, O. Kasian, M. Ledendecker, E. Pizzutilo, A. M. Mingers, W. T. Fu, O. Diaz-Morales, Z. Li, T. Oellers, L. Fruchter, A. Ludwig, K. J. J. Mayrhofer, M. T. M. Koper, S. Cherevko, *Nat. Catal.* **2018**, *1*, 508–515.
[47] D.-J. Chen, B. Xu, S.-G. Sun, Y. J. Tong, *Catal. Today* **2012**, *182*, 46–53.
[48] J. Álvarez-Malmagro, F. Prieto, M. Rueda, A. Rodes, *Electrochim. Acta* **2014**, *140*, 476–481.
[49] A. Lobo, H. Conrad, *Surf. Sci.* **2003**, *523*, 279–286.
[50] K. Du, L. Zhang, J. Shan, J. Guo, J. Mao, C.-C. Yang, C.-H. Wang, Z. Hu, T. Ling, *Nat. Commun.* **2022**, *13*, 5448.

Manuscript received: July 19, 2024
Accepted manuscript online: August 12, 2024
Version of record online: ■■, ■■

Research Article

Acidic Water Electrolysis

Y. Duan, L.-L. Wang, W.-X. Zheng, X.-L. Zhang,* X.-R. Wang, G.-J. Feng, Z.-Y. Yu,* T.-B. Lu* ______________ **e202413653**

Oxyanion Engineering on RuO_2 for Efficient Proton Exchange Membrane Water Electrolysis

MoO_3 stabilizing sulfate on RuO_2 for efficient PEMWE

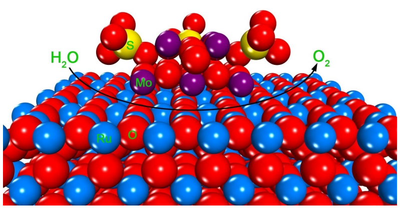

An anion modification strategy has been developed to improve the acidic OER performance of RuO_2 by MoO_3-stabilized sulfate anion, which exhibits the exceptional OER activity and stability in both acidic electrolyte and proton exchange membrane water electrolysis.